Coupling Underwater Superoleophobic Membranes with Magnetic Pickering Emulsions for Fouling-Free Separation of Crude Oil/Water Mixtures: An Experimental and Theoretical Study

Alexander V. Dudchenko, Julianne Rolf, Lucy Shi, Liana Olivas, Wenyan Duan, and David Jassby*

Department of Chemical and Environmental Engineering, University of California, Riverside, California 92521, United States

ABSTRACT Oil/water separations have become an area of great interest, as growing oil extraction activities are increasing the generation of oily wastewaters as well as increasing the risk of oil spills. Here, we demonstrate a membrane-based and fouling-free oil/water separation method that couples carbon nanotube–poly(vinyl alcohol) underwater superoleophobic ultrafiltration membranes with magnetic Pickering emulsions. We demonstrate that this process is insensitive to low water temperatures, high ionic strength, or crude oil loading, while allowing operation at high permeate fluxes and producing high quality permeate. Furthermore, we develop a theoretical framework that analyzes the stability of Pickering emulsions under filtration mechanics, relating membrane surface properties and hydrodynamic conditions in the Pickering emulsion cake layer to membrane performance. Finally, we demonstrate the recovery and recyclability of the nanomagnetite used to form the Pickering emulsions through a magnetic separation step, resulting in an environmentally friendly, continuous process for oil/water separation.

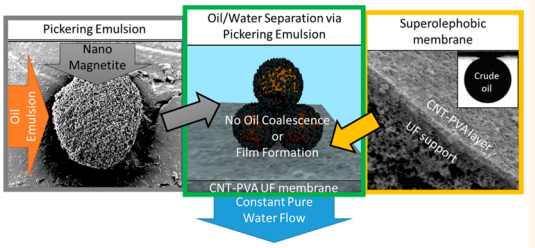

KEYWORDS: Pickering emulsion · ultrafiltration · underwater superoleophobic membranes · fouling prevention · oil/water separation

Over the last 30 years, the demand for fossil fuels has dramatically increased, with growing demand projected to increase well into the future.[1,2] The extraction of crude oil leads to a potential for large oil spills, such as seen during the Deepwater Horizon disaster.[3] Furthermore, modern extraction processes generate large volumes of complex oily wastewater, known as produced water, which contain oil (free and emulsified), surfactants, and minerals.[4] The free oil and oil emulsions that are present in produced water, as well as generated during oil spills, pose a significant hazard to the environment.[5,6] This hazard has created a pressing need to develop an effective method of treatment, with the majority of recent work exploring novel materials that exhibit superhydrophobicity/superoleophilicity or superhydrophilicity/underwater superoleophobicity.[7−19]

Superhydrophilic/underwater superoleophobic membranes and meshes have been developed to physically separate oil from water, with the goal of minimizing membrane fouling and increasing oil rejection.[7−13] Membrane fouling from oil, where oil clogs membrane pores, is a common problem in membrane separation of oil emulsions.[20,21] Although some filtration techniques have demonstrated excellent oil removal, a majority of studies do not present fouling data or demonstrate whether the membranes suffer from fouling.[10,11] Superhydrophobic/superolephilic foams and meshes have been synthesized for chemical and physical sorption of oil from water, showing good separation and sorption performance, but they still have to overcome scale-up challenges, use of costly materials, and complicated fabrication procedures.[14−19] Magnetic Pickering emulsions have also been

* Address correspondence to djassby@engr.ucr.edu.

Received for review June 5, 2015 and accepted September 30, 2015.

Published online September 30, 2015
10.1021/acsnano.5b04880

proposed for oil/water separation. Here, oil emulsions are stabilized with magnetic nanoparticles (NPs), which are removed from the water through the application of a magnetic field.[22−25] However, the use of magnetic fields poses a big challenge for scalability, as the magnetic field strength drops with an inverse cubed law, thus requiring a large magnetic surface area to effectively treat the vast volumes of fluids collected during oil spills.

Herein, we describe a novel method of oil/water separation by coupling carbon nanotube−poly(vinyl alcohol) (CNT−PVA) underwater superoleophobic ultrafiltration (UF) membranes to magnetic Pickering emulsions. In this approach, the Pickering emulsions are used to prevent oil coalescence in the cake layer that forms on the membrane surface during filtration, while underwater superoleophobicity prevents membrane wetting and consequent fouling. We demonstrate how water contaminated with large amounts of crude oil (up to 10% by volume) can be effectively treated with UF membranes without the extreme fouling typically observed in this process while producing a permeate stream with less than 15 ppm of total organic carbon (TOC) (regardless of the oil concentration in the feed). We further develop a theoretical framework that describes the interaction of NP-stabilized oil (*i.e.*, a Pickering emulsion) with a porous surface (*i.e.*, a UF membrane) under filtration mechanics. The framework considers the interaction energy between the oil/NPs and oil/surface as a function of pressure gradients typical in membrane separation processes. Furthermore, we demonstrate how the NPs can be magnetically recovered from the concentrated Pickering emulsions, allowing for their reuse in another round of oil/water separation. The robust and sustainable water treatment process described here is insensitive to crude oil concentrations (tested with concentrations up to 10% v/v oil/water), temperature, ionic strength and species, and can be used for the separation and recovery of oil from wastewater and during oil-spill remediation activities.

RESULTS AND DISCUSSION

Characterization of Oil and Pickering Emulsions. We have developed a novel method of oil/water separation using Pickering emulsions coupled to underwater superoleophobic ultrafiltration membranes. Crude oil emulsions were prepared by using a simple blending process, which formed polydisperse oil droplets with a majority of droplets having a diameter bellow 6 μm (Figure 1a,c). The small, emulsified crude oil droplets are potent foulants; during filtration they can coalesce to form oil films on the membrane surface and/or deform and penetrate into the membrane pores, which results in irreversible membrane fouling and rapid performance decline.[21,26,27] Oil coalescence can be prevented *via* Pickering emulsions, which have been of great interest as they are capable of stabilizing large concentrations of oil in water.[24,28−32] Pickering emulsions were prepared with Fe_3O_4 nanopowder (FeNPs) and polyvinylpyrrolidone-coated Fe_3O_4 nanopowder (FePVP) that had a water contact angle of 40 ± 3 and 6.8 ± 1°, respectively (Figure S1). FeNP and FePVP both had a primary particle size of 20−40 nm. However, due to their ferromagnetic qualities, these particles form aggregates with a diameter of 608 ± 7 and 727 ± 40 nm, respectively, as determined by dynamic light scattering (DLS). The Pickering emulsions were prepared *via* a simple mixing process where 10 g/L of FeNPs or FePVPs was added to 10 mL/L of emulsified crude oil and mixed with a paddle mixer for 1 and 3 h, respectively (Figure 1b,c). The longer mixing time was needed for FePVP due to their very hydrophilic nature (water contact angle of 6.8 ± 1°) that leads to a small energy well for entering the water/oil interface (165 kT) compared to FeNPs that had a contact angle of

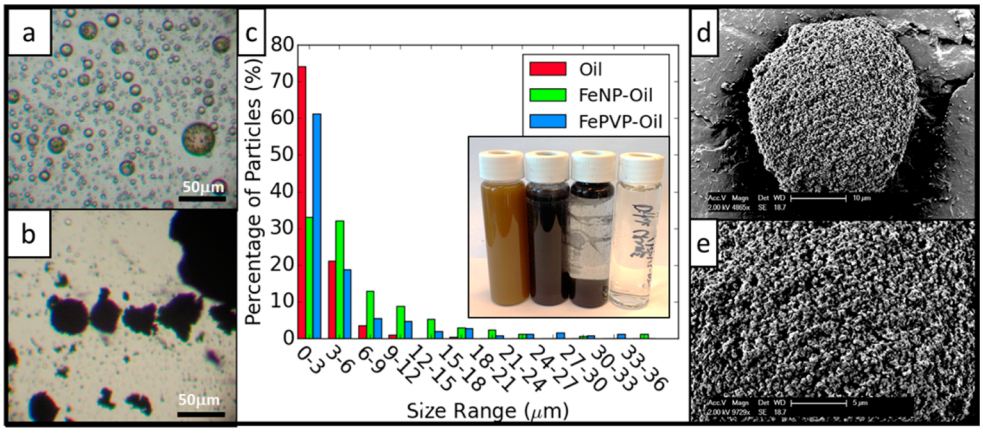

Figure 1. Images of oil and Pickering emulsions. (a) Image of a typical (nonstabilized) crude oil emulsion. (b) Image of FeNP Pickering emulsions. (c) Size (diameter) distribution of oil and Pickering emulsions; (inset) vial contents are from left to right: 10 mL/L crude oil emulsion, 10 mL/L Pickering emulsion, gravity separated 10 mL/L Pickering emulsion, and UF permeate with <15 ppm TOC. (d) SEM image of NP-stabilized oil drop. (e) Higher resolution image of magnetic NPs on the surface of the oil drop.

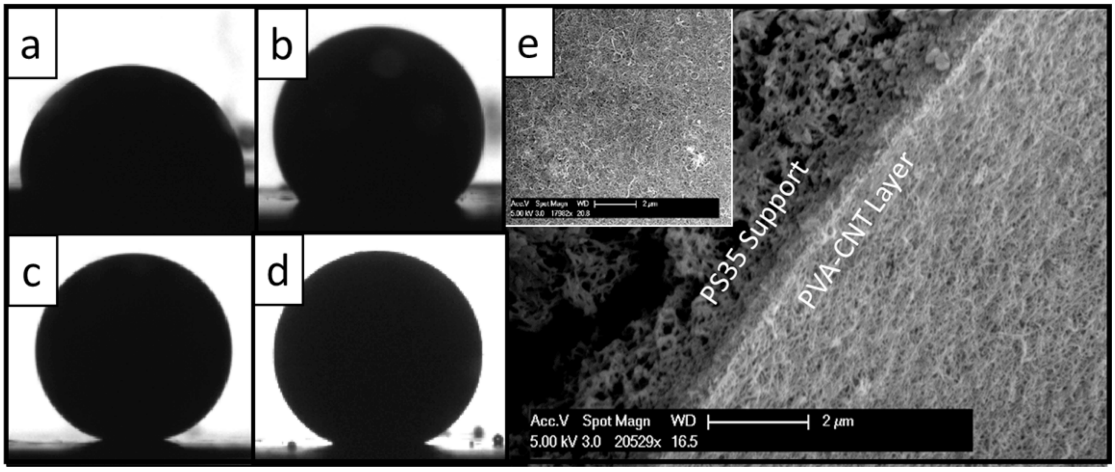

Figure 2. Underwater contact angles of crude oil drops with the membrane surface after 20 min on (a) PS35 with contact angle of 100 ± 2°, (b) PAN with contact angle of 130 ± 2°, (c) PVA-CNT with contact angle of 168 ± 2°, and (d) PS35 with FeNP-stabilized crude oil drop and contact angle of 155 ± 2°. (e) Cross-sectional SEM image of PVA-CNT membrane on PS35 support; (inset) top surface of the PVA-CNT layer showing the overall smoothness of the membrane.

40 ± 3° and an energy well of ~1.8 × 10^5 kT (calculated for surface tension 0.05 N m^{-1} and an oil drop with a radius of 3.3 μm) (Figures S1, S2).[33]

The FeNP and FePVP-stabilized oil droplets had a similar size distribution compared to the unstabilized crude oil emulsion; the FePVP-stabilized oil is slightly smaller, with nearly 60% of droplets having a diameter bellow 3 μm (Figure 1b,c). The formation of larger droplets that are not observed in the pure crude oil emulsions is attributed to the ferromagnetic properties of NPs, which aggregate smaller droplets. Scanning electron microscopy (SEM) image analysis further confirms the presence of a dense FeNP coating on the surface of the oil droplets, which form a protective layer at the oil/water interface (Figure 1d,e). The Pickering emulsions were extremely stable, and did not phase-separate into oil, water and NP phases even after several months of storage at room temperature. After prolonged periods, a large fraction of the NP-stabilized oil settles out, with a smaller fraction remaining suspended at the top of the aqueous phase, likely due to creaming (Figure 1c, inset); the aqueous phase had no visible oil, with a TOC of 13 ± 7 ppm (as measured with a TOC analyzer), which further demonstrates that all of the oil was trapped in a Pickering emulsion.

Oil/Water Separation. The fouling propensity of the NP-stabilized oil drops was investigated on a range of membrane materials that had different hydrophilic surface properties. The membrane materials included two commercially available UF membranes made of polysulfone (PS35) and polyacrylonitrile (PAN), and two modified UF membranes with poly(vinyl alcohol) carbon nanotube coating (PVA-CNT) on PS35 (PS35-CNT) and PAN (PAN-CNT). The PVA-CNT coating deposited on the PS35 or PAN support governs the membrane surface properties, including hydrophilicity, but does not influence their rejection properties or permeability, as demonstrated by Dudchenko *et al.* (2014) (Figure 2e).[34] The tendency of the membranes to become wet by oil was measured by allowing a crude oil drop to contact the membrane in a water-filled inverse cell, and measuring the contact angle over a 20 min period. After 20 min, the contact angles were 100 ± 2, 130 ± 2, and 168 ± 3°, for the PSF, PAN, and PVA-CNT membranes, respectively, with smaller angles corresponding to a more hydrophobic surface that is more readily wetted by the oil (Figure 2a−c and Figure S3). The high contact angle of the PVA-CNT membranes with oil demonstrates their underwater superoleophobic properties; however, their contact angle with oil in air was below 30°. When an FeNP coated oil drop was allowed to come in contact with the hydrophobic PS35 membrane, the contact angle increased from 100 ± 2° (the bare oil drop on the PS35 membrane) to 155 ± 2° (Figure 2d and Figure S3), which clearly demonstrates that a coating of FeNPs greatly reduces the ability of an oil drop to wet a surface by preventing physical contact between the crude oil and the membrane surface.

Although PVA-CNT membranes demonstrate excellent underwater superoleophobicity, they are still prone to a high degree of fouling when filtering pure oil emulsions (0.5 mL/L of crude oil in deionized water (DIW)) (Figure S4). Under these conditions, flux step experiments[35−37] demonstrate that when the membranes operate at fluxes below 30 L/(m^2 h) (LMH) the membranes experienced fouling rates of 2−5 psi/h; when operated at higher fluxes, the membranes rapidly fouled with flux declines exceeding 10 psi/h (Figure S4). These fouling results indicate that even at low permeate fluxes and oil concentrations, the membrane rapidly fouls, demonstrating that underwater superoleophobicity is not sufficient to treat water contaminated by emulsified crude oil. This finding demonstrates the complexity of treating water contaminated with crude

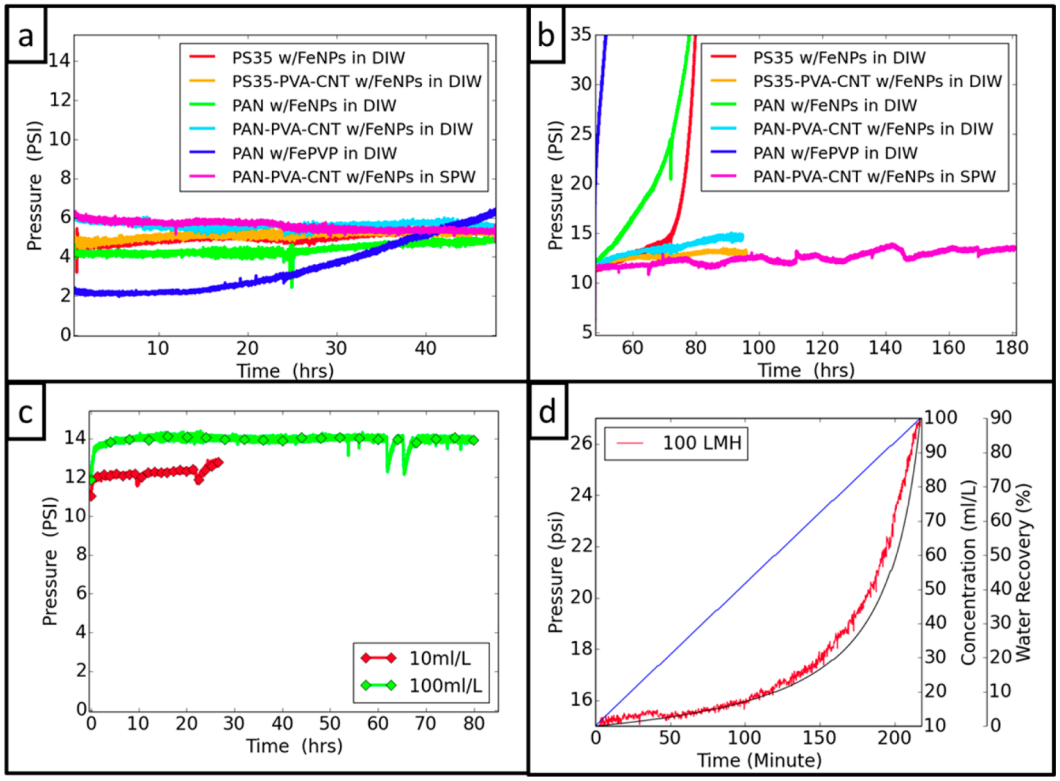

Figure 3. Membrane performance while treating NP-stabilized crude oil. (a) Membrane performance at 50 LMH with a cross-flow velocity of 15 cm/s. (b) Membrane performance at 100 LMH with a cross-flow velocity of 15 cm/s. (c) Fouling of PS35-PVA-CNT membrane in SSW at 2 °C with a cross-flow velocity of 25 cm/s with two crude oil concentrations (10 and 100 mL/L). (d) Concentration experiment on PS35-PVA-CNT membrane at 100 LMH in SSW at 2 °C with a cross-flow of 10 cm/s; the blue line is water recovery (%), the black line is crude oil concentration (in ml/L), and the red line is the system pressure.

oil, and indicates that underwater superoleophobic membranes alone are not capable of preventing membrane fouling.

To overcome the limitations imposed by the extreme fouling observed during the filtration of pure crude oil emulsions, we use Pickering emulsions to improve system performance. We performed fouling experiments at a constant permeate flux of 50 and 100 LMH with a cross-flow velocity (CFV) of 15 cm/s, using FeNP and FePVP stabilized Pickering emulsions. In the first set of experiments, crude oil in DIW (10 mL/L) was stabilized with 10 g/L of NPs. At a constant permeate flux of 50 LMH, FeNPs-stabilized oil emulsions formed in DIW demonstrated no fouling, regardless of the membrane used (Figure 3a). In contrast, the use of FePVPs-stabilized oil in DIW resulted in rapid fouling (Figure 3a). At a constant permeate flux of 100 LMH, the FeNPs-stabilized emulsions in DIW were able to foul the PS35 and PAN membranes. However, the PVA-CNT coated membranes continued to demonstrate excellent performance, with limited observable fouling over a period of 48 h (Figure 3b). Not surprisingly, the FePVP-stabilized oil in DIW rapidly fouled the membranes at a flux of 100 LMH (Figure 3b). In all cases, the TOC content in the membrane permeate was below 15 ppm, indicating an oil removal efficiency exceeding >99.7%.

The stability of the Pickering emulsions (10 mL/L of crude oil stabilized with 10 g/L of FeNPs) and the fouling resistance of PVA-CNT membranes were further challenged with high ionic strength conditions, using a synthetic produced water (SPW) with an ionic strength of 2.24 M.[4] This water contained the most common ions present in produced waters, including a high loading of the divalent cations Ca^{2+} and Mg^{2+}, with a molar concentration of 0.171 and 0.169 M, respectively. It was hypothesized that these divalent ions would lead to the complete collapse of any repulsive electrostatic forces between the NPs and oil drops, and possibly allow for bridging between the membrane surface and the Pickering emulsions, leading to rapid fouling. However, even after continuous operation for 48 h at a permeate flux of 50 LMH and 180 h at permeate flux of 100 LMH, no fouling was observed (Figure 3a,b). The lack of membrane fouling even under these harsh conditions indicates that electrostatic forces do not play a significant role in the stability of this system, and that divalent ionic bridging does not occur.

Since oil becomes more viscous at lower temperatures, and considering the increased probability of arctic oil drilling (and hence the increased probability of an arctic oil spill), the effect of temperature on system performance was also explored. Experiments

were performed in synthetic seawater (SSW) at a temperature of 2 °C. Long-term experiments were performed with a crude oil loading of 10 and 100 mL/L on a PS35-PVA-CNT membrane (CFV 25 cm/s). The reduced temperature had no impact on membrane performance, with no membrane fouling observed even at the high oil loading of 100 mL/L over a period of 80 h (Figure 3c). Finally, concentration experiments were used to determine the maximum water recovery possible, where a Pickering emulsion with a concentration of 10 mL/L of crude oil was concentrated to 100 mL/L of crude oil using PS35-PVA-CNT membrane (Figure 3d, CFV 10 cm/s). In this experiment, membrane permeate was not returned to the feed tank, and the concentration of crude oil in the feed was allowed to increase. The PVA-CNT membranes again demonstrated excellent performance, and no fouling was observed at 90% recovery, with the observed pressure increase correlating nearly perfectly to the increase in crude oil concentration. These fouling experiments demonstrate that Pickering emulsions coupled to a UF treatment system provide a highly effective method for the treatment of oily waters. Excellent performance was observed regardless of the ionic strength, ionic species, temperature, or oil concentrations (within the limits of our testing), demonstrating the robustness of the treatment method even under highly challenging conditions, with excellent oil removal rates (>99.7 and >99.9% rejection at 10 and 100 mL/L crude oil loading, respectively).

The impact of the FeNPs on the structural properties of the oil and Pickering emulsion droplets was explored through force probing using an atomic force microscope (AFM). The results indicate that the stiffness of the crude oil drops does not change significantly with the addition of FeNPs, as implied by the near identical slopes of the force line generated during the retraction of the AFM probe (Supplemental Section S1).[38] The AFM study did reveal the presence of a layer of FeNP at the oil/water interface, and it was further found that the FeNPs seem to rearrange as the tip is used to repeatedly probe the surface of the drop, indicating a mobile NP layer (Supplemental Section S1, Figure S7a,b). These results suggest that under pressure the NP-stabilized oil drops will deform similarly to uncoated oil drops, and that the stiffness of the NP-stabilized oil drop does not impact membrane fouling, as demonstrated by the fouling experiments.

The deposition and attachment of NPs to the membrane surface can also lead to fouling.[39−41] The lack of fouling during the filtration of FeNP stabilized oil (with DI or SPW waters) indicates that the FeNPs do not deposit or sorb to the membrane surface. However, the FePVP stabilized oil did foul the membrane, which could be attributed to the FePVP particles themselves adsorbing to, and blocking, the membrane surface. Particles coated with PVP have been previously shown to preferentially attach to non-PVP coated surfaces under moderate ionic strength conditions.[42] However, membranes used during the FePVP stabilized oil separation experiments were made of PAN, which has PVP added to it during their manufacturing process.[43,44] Thus, the presence of PVP coating on PAN membranes and the low ionic strength during the FePVP experiments (DIW) would prevent preferential sorption of FePVPs to the membrane surface, and mitigate attachment of the FePVP particles to the membrane surface. Since fouling still occurred during these conditions, it can likely be attributed to oil coalescence. This information indicates that under the current experimental conditions, membrane performance when filtering FeNP/FePVP-stabilized oil is controlled by permeate flux, membrane oleophobicity, and NP contact angle, and not by specific interactions between the NPs and the membrane surface.

Theoretical Analysis of Experimental Results. Our experimental results demonstrate that oil droplets stabilized with FeNPs will not foul the membranes under our reported experimental conditions. The NPs prevent direct oil−oil interaction between adjacent oil drops as well as oil−membrane interactions, which prevents drop coalescence as well as membrane wetting by the oil.[22−25] The theoretical framework we developed connects the force that holds the NPs at the oil/water interface to forces resulting from the crossflow filtration of the emulsion (detailed explanation in Supplemental Section S2). The force that holds the NPs at the oil/water interface of a Pickering emulsion is a result of surface energy minimization (*i.e.*, interfacial energy) (equation S1).[45,46] The interfacial energy can be used to calculate the force that holds the particles in place (Figure 4a) (Supplemental Section S2.2, equations S2−S3). This allows us to perform a force balance, which determines if the particle will remain at the interface under various forces acting on the system during filtration (*e.g.*, pushing, pulling or rolling force) (Figure 4b).

The model first considers the stability of the Pickering emulsion in a cake layer that formed on the membrane surface during cross-flow filtration. The cake layer is a complicated structure that generates a large number of forces that act on the Pickering emulsion and membrane surface. We first consider the forces that prevent oil coalescence, as coalescence would lead to membrane fouling. The force profiles acquired from the AFM study demonstrate that the NP layer on the oil drop surface is mobile, and moves under the application of an external force (Supplemental Section S1). Thus, forces resulting from fluid flow through the cake layer could potentially cause NP movement along the oil drop surface, which can lead to oil from neighboring drops to coalesce and lead to fouling. The model then assumes the presence of two NPs that are placed between two oil drops, preventing

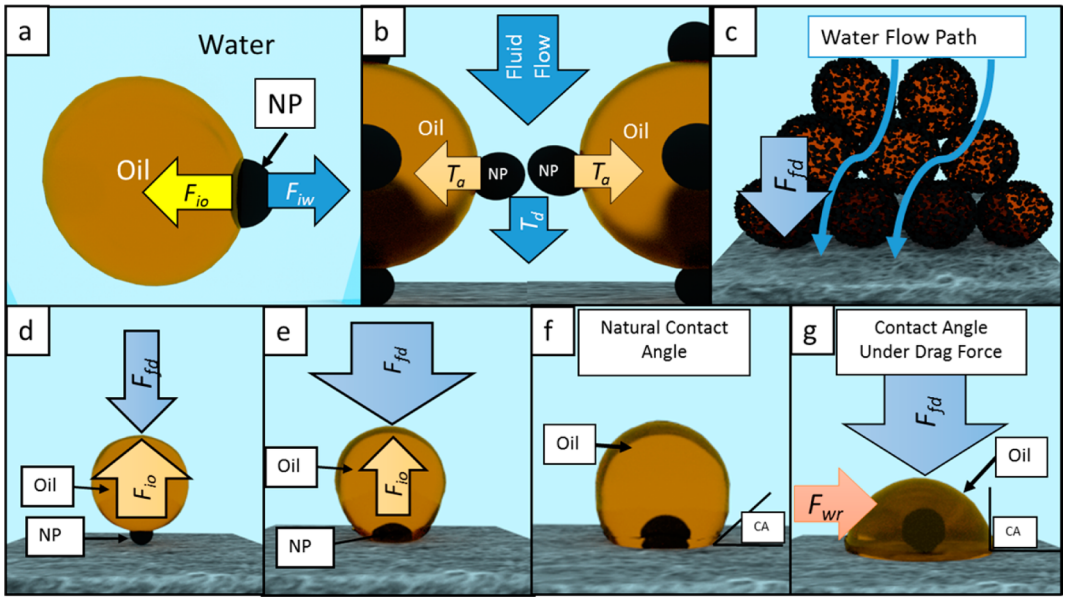

Figure 4. (a) The model uses a single NP at the oil/water interface to calculate the force required to either pull the NP out of the drop (F_{iw}) (blue arrow) or push the NP into the oil drop (F_{io}) (yellow arrow). (b) The shearing forces acting on the NPs in the cake layer are shown; the fluid flow through the cake layer generates a rolling torque that acts on the particles (T_d), with an adhesive torque (T_a) (holding the particle in place) preventing the particle from rolling off the oil surface. (c) The flow through the cake layer results in a nonlinear flow path, which exerts a drag force (F_{fd}) on the surface of the Pickering emulsion drops. The drag force transfers from the top layer to the bottom layer, leading to a force (F_{fd}) that has to be supported by the lowest Pickering emulsion drops in the cake layer. (d) The drag force (F_{fd}) pushes the oil drop into the NP, and the interfacial force (F_{io}) acts against it, preventing oil from coming in contact with the membrane. (e) When the drag force (F_{fd}) is stronger than interfacial force (F_{io}), the NP enters the oil phase, allowing oil to come in contact with membrane. (f) When oil comes in contact with membrane, it wets the surface to the oil's natural contact angle with the membrane surface. (g) The oil spreads due to the drag force (F_{fd}), leading to a higher contact angle than the natural contact angle, which leads to further membrane wetting and fouling.

the oil in adjacent drops from interacting (Figure 4b). The fluid drag through the cake layer would result in a rolling torque (T_d) that would try to roll the particle off the oil surface (equations S4, S8−S10).[47−51] An interfacial force (F_{iw}) that holds the NP at the oil/water interface generates an adhesive torque (T_a) that prevents the particle from rolling off the surface (equations S5−S7).[45,47,49] If the particles were to roll off the oil drop surface, the oil in neighboring drops would be exposed, which would lead to coalescence and fouling. Thus, a simple torque balance allows us to determine if coalescence would occur. In our model, if a coalescence event occurs, then we assume the membrane will foul. A detailed procedure for the calculation of the torque balance is presented in Supplemental Section S2.3.

The fluid flow through the porous structure of a cake layer leads to a drag force (F_{fd}), which has to be supported by the Pickering emulsion structure, and in particular, by the bottom layer of the Pickering emulsion that is in contact with the membrane (Figure 4c). The fouling here is mitigated by a layer of NPs that prevent oil from coming in contact with the membrane surface. A force balance is then performed around a single NP that separates the oil drop from the membrane surface (Figure 4d). The interfacial force (F_{io}) that holds the particle at the oil/water interface has to resist the drag force acting on the cake layer, preventing the particle from entering the oil phase (equations S3b, S11). If the drag force through the cake layer is lower than the interfacial force holding the particle at the oil/water interface, then the membrane will not foul. Otherwise, the oil can come into contact with the membrane, and we must consider the susceptibility of the membrane material to wetting (Figure 4e). A detailed procedure for calculating the forces acting on a particle separating the oil from the membrane is presented in Supplemental Section S2.4.

The drag force acting on the cake layer can force the oil drops to be exposed to the membrane surface and come directly in contact with it. The oil can then wet the membrane surface to its natural energetic minimum (*i.e.*, its measured contact angle); further membrane wetting requires an external force to be applied to the drop (Figure 4f,g). In the cake layer, a drag force (F_{fd}) provides this external force, which acts against the membrane natural resistance to wetting (F_{wr}); if $F_{fd} > F_{wr}$, then the oil is forced to spread further across the membrane surface (Figure 4g) (equations S11−S14).[52] We assume that to completely wet the membrane, a contact angle of 90° is required, since at this angle oil from adjacent drops would come in contact at the edges, which would then lead to coalescence and fouling. A detailed procedure for calculating the force

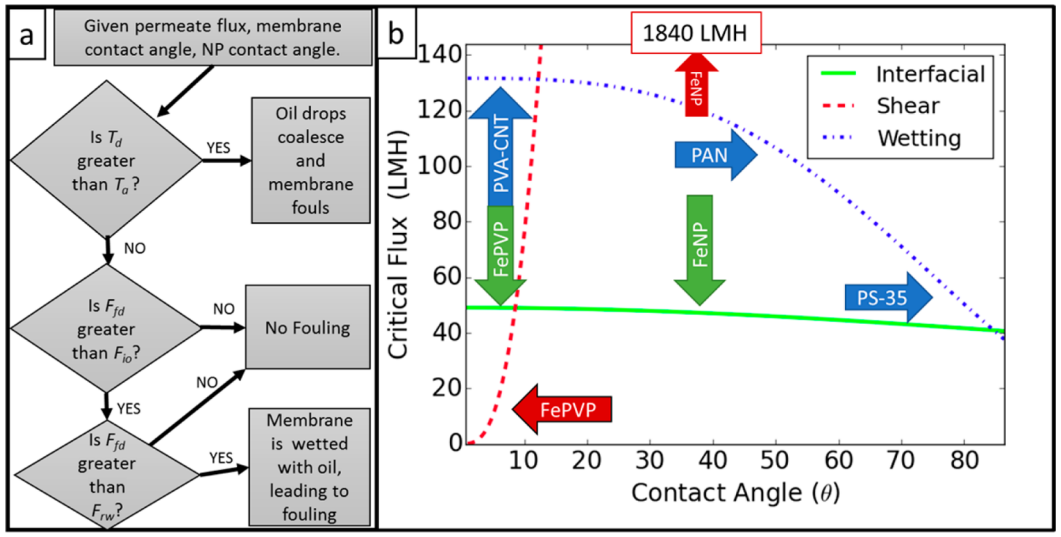

Figure 5. (a) Theoretical framework flowchart. (b) Model results demonstrating the relationship between the critical permeate flux (*y* axis) and membrane and NP contact angle (*x* axis): the interfacial (green) line shows the solution to the force balance for the fluid drag force (F_{fd}) and the interfacial force (F_{io}), while the shear (red) line represents the torque balance between the fluid drag torque (T_d) and the torque of adhesion (T_a). Both lines are showing a solution for the critical flux *vs* NP contact angle. The wetting (blue) line shows the force balance between the fluid drag force (F_{fd}) and the membrane wetting resistance (F_{wr}), solved for the critical flux *vs* membrane contact angle. The PVA-CNT, PAN, and PS-35 arrows point to the membrane contact angles, and the FePVP and FeNP arrows point to the NP contact angles.

balance and determining oil spreading is presented in Supplemental Section S2.5.

The overall model can then be solved in several steps (Figure 5a) if the following information is known: the contact angle of the NPs with oil and water; the contact angle of the membrane with oil; the permeate flux and pressure drop across the cake layer (Figure 5a). The first step in the model is to determine if coalescence in the cake layer would take place. If coalescence does occur, then the membrane will foul under the specified conditions. If coalescence does not occur, then it is determined if the drag force through the cake layer is sufficient to push the NPs into the oil drop, which leads to the oil coming in contact with the membrane surface. If the oil does not come in contact with the membrane surface, then no fouling occurs. If the oil comes in contact with the membrane surface, then it has to be determined if the membrane will be wetted with oil, which would lead to membrane fouling. This simple theoretical framework allows for the determination of the important operational conditions under which the membrane could foul. A detailed description of this process is presented in Supplemental Section S2.6.

Model Results. The theoretical framework developed for this work successfully captured the relationship between Pickering emulsion stability, membrane oleophobicity, and permeate flux. Experimental results demonstrate the significant difference between the FeNP and FePVP-stabilized oil drops under filtration conditions (Figure 3a,b), which prompted the investigation of the stability of the NPs at the oil/water interface. Thus, the first step is to understand the relationship between NP contact angle and Pickering emulsion stability when exposed to the shear forces found in the cake layer accumulated on the membrane surface, with the goal of finding the flux point where membrane fouling would occur (*i.e.*, the critical flux). Model results (generated using equations S1−S10) indicate that NPs with water contact angles <10° readily shear off the oil/water interface, leading to oil drop coalescence and membrane fouling, at fluxes above 40 LMH. Thus, the FePVP particles (with a contact angle of 6.8°) shear off at fluxes exceeding 26 LMH (critical flux of 26 LMH) (Figure 5b). In contrast, the FeNP particles, having a water contact angle of 40°, are very resistant to shear forces, requiring a flux of 1840 LMH to be sheared away from the oil/water interface (Figure 5b). To verify the framework results, additional experiments were performed using γ-Fe_2O_3 (γ-FeNP) and polystyrenesulfonate modified γ-FeNP (FePSS) nanoparticles with contact angles of 10 ± 2° (critical flux of 76 LMH) and <5° (critical flux of 12 LMH), respectively (Figures S1 and S5). The experiments revealed that FePSS stabilized oil fouled in a very short time when operating at 50 LMH, while the γ-FeNP stabilized oil began fouling at operating flux of 80 LMH, demonstrating the reliability of the proposed theoretical framework. Thus, during filtration experiments it is likely that the shear forces in the cake layer stripped the FePVP from the oil drops, allowing the membrane to foul (Figure 3a). However, these forces were insufficient to remove the FeNPs from the oil/water interface, which leads to the conclusion that another mechanism is responsible for the observed fouling at 100 LMH on the relatively oleophilic PS35 and PAN membranes (Figure 3b).

Using equations S1−S3 and S11, we found that the pressure drop across the cake layer in our system would cause the FeNPs separating the oil from the membrane to be "pushed" into the oil drop itself, and allow the oil to come into contact with the membrane, when fluxes exceeded 48 and 46 LMH for the FePVP and FeNP, respectively (Figure 5b). The slightly higher critical flux for FePVP is due to their higher hydrophilicity, which increases the energy barrier preventing the FePVP particle from partitioning into the oil drop. The relatively small change in the critical flux is due to the fact that the total difference between the energy barriers is relatively small compared to the overall energy barrier (1.346×10^7 *vs* 1.365×10^7 kT for FeNP and FePVP, respectively, Figure S1). This higher energy for partitioning into the oil also leads to a smaller energy barrier existing for the particle to be pulled out of the oil drop. However, this difference is very significant with the energy barrier being 165 kT for FePVP and 1.83×10^5 kT for FeNP (Figure S1). Equations S11−S14 were used to determine whether the membrane material, once in contact with the crude oil (if the NPs at the oil/membrane interface are pushed into the oil drop itself), would wet. To do so, F_{wr} was compared to the force experienced by the bottom-most oil drop in the cake layer (derived from the pressure drop across the cake layer, F_{fd}). The results of the model demonstrate that the critical flux for the PVA-CNT membranes is 131 LMH, which would lead to no fouling at fluxes of 50 and 100 LMH, as was experimentally observed (Figure 5b). The critical flux for PAN and PS35 was found to be 105, and 50 LMH, respectively, with experimental results demonstrating fouling at 100 LMH for both membranes (Figure 3a,b).

Finally, the results of the various model components can be compared to our experimental results using the theoretical framework described in Figure 5a, for the purpose of understanding the mechanisms responsible for the observed fouling phenomena. Since the PAN membrane fouled when treating the FePVP-stabilized oil at 50 LMH but not when treating the FeNP-stabilized oil, it is likely that the fouling mechanism involved the shearing of the FePVP particles from the oil/water interface, as predicted by the model (Figure 3a,b). At higher fluxes (100 LMH), the PS35 and PAN membranes both rapidly fouled, in contrast to the PVA-CNT membranes, which are significantly more oleophobic, that did not foul (Figures 2 and 5b). The model predicts that the relatively hydrophobic PS35 and PAN membranes will become wetted by the crude oil if the oil comes into contact with the membrane surface at fluxes of ~100 LMH. Furthermore, the model predicts that at a flux of 100 LMH, the force acting on the cake layer is sufficient to push the NPs into the crude oil drop, thus allowing contact between the oil and membrane surface. Therefore, the mechanism responsible for the fouling of the PS35 and PAN membranes at 100 LMH is wetting by the oil. Additionally, the mechanism responsible for the fouling of the PVA-CNT membranes when filtering the bare oil emulsions (no NPs; Figure S4) is the lateral coalescence of oil drops in the cake layer, since there are no NPs separating neighboring drops.

Nanoparticle Recovery and Reuse. The magnetic properties of the NPs used to prepare the Pickering emulsions provide an opportunity to recover the NPs from the concentrated crude oil in the membrane concentrate stream, through the application of an external magnetic force. It has been previously demonstrated that Pickering emulsions prepared with micron-sized particles could be easily separated from oil using a strong magnetic force.[22] However, it was also found that NPs adhere strongly to the oil/water interface and do not undergo spontaneous separation like their larger counterparts.[23] We found that the Pickering emulsion can be readily separated from the aqueous phase using a strong magnet (N48 rare earth magnet). Following exposure to air, the oil readily seeps out under gravity, leaving the NPs attached to the magnet (Figure 6a). However, gravity separation was found to be insufficient for FeNP reuse due to significant amounts of

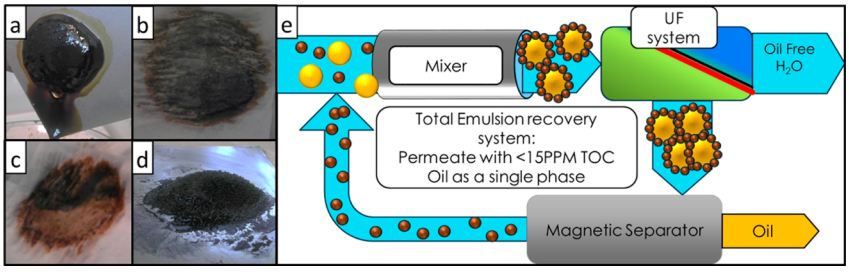

Figure 6. Magnetic NP recovery process: (a) after the Pickering emulsion is recovered from water and exposed to air, oil readily seeps from the NPs. (b) Blotting paper used to wick oil from the NPs. (c) Oil that was wicked out of FeNPs is shown on the blotting paper. (d) Recovered nanoparticles are seen in their dry-like state. (e) Complete oil emulsion treatment system: starting from the top left, oily water enters a mixer with FeNPs to form a Pickering emulsion; the Pickering emulsion enters the UF system, where it is concentrated to produce an oil-free permeate stream, and a concentrated stream; the concentrated Pickering emulsion is passed into a magnetic separator, which separates water and FeNPs from oil, producing an oil stream and an FeNP slurry that is reused for the formation of a new Pickering emulsion (brown dots are FeNPs and large yellow dots are oil droplets).

oil remaining in the FeNP slurry (70−80%), which prevented their effective dispersion in water. Thus, a wicking step was added to the separation and recovery process, where the oil was wicked out of the FeNPs using blotting paper (Figure 6b,c). This approach reduced the oil content in the FeNP slurry to 31 ± 6% of the initial crude oil weight, producing a nearly dry FeNP powder that readily formed new Pickering emulsions (Figure 6d). The process of recovery and reuse was repeated three times, with no apparent drop in the FeNP's ability to form new Pickering emulsions. The recovery and reusability of FeNPs allows for the development of a continuous, membrane-based and fouling-free oily water treatment process. Such a process would stabilize oil emulsions with FeNPs, forming Pickering emulsions that would be concentrated with UF, producing oil-free water. The concentrated Pickering emulsions would then go through a magnetic separation process producing a FeNP slurry that could be reused (*i.e.*, form new Pickering emulsions), and a highly concentrated oil stream (Figure 6e).

CONCLUSIONS

The coupling of Pickering emulsions to underwater superoleophobic UF membranes allows for a rapid and robust oil/water separation method (up to 100 LMH) for water contaminated with large quantities of crude oil (up to 100 mL/L) with minimal fouling. The novel process reported here is insensitive to solution ionic strength (>2 M), temperatures (2−25 °C), and produces treated water with a TOC content <15 ppm regardless of oil concentrations in the feed. The 15 ppm threshold is critical, as this is the level considered acceptable for environmental discharge for treated water.[53] The developed theoretical framework and model explain our experimental results, indicating that fouling inhibition is due to the noncoalescing nature of Pickering emulsions as well as membrane underwater superoleophobicity that prevents oil wetting of the membrane surface. Importantly, our work demonstrates that an underwater superoleophobic membrane alone is insufficient to prevent membrane fouling under realistic conditions. Finally, we have demonstrated that crude oil could be separated from FeNPs using an external magnetic field coupled to a wicking process, which allows for their recovery and reuse.

The process developed here has significant implications for oily water treatment, as it allows for rapid handling of concentrated oil streams, while producing very high quality treated water, without experiencing membrane fouling. The advantage of UF over other oil/water separation techniques is the tight membrane pore size, which guarantees an oil-free permeate that can be easily reused or disposed of. The fact that the system does not foul will prevent excess costs associated with UF cleaning and process interruption. Membrane fouling leads to increased power demands with the expected power usage for nonfouled membranes being less than 0.2 kWh/m^3 or \$0.013/m^3 (based on average industrial power cost in the USA in 2014).[54,55] The addition of CNTs to fabricate the underwater superolephobic membranes used in this study incurs a relatively minor additional cost of \$2.21/m^2, which amounts to an 11% increase compared to the cost of the PS35 polysulfone membrane material. Finally, we estimate that the energetic cost of magnetic separation would only be 0.00411 kWh/m^3 (0.000275 \$/m^3), amounting to less than 2% of total energy consumption (based on MSK-300 magnetic separator (PRAB, Kalamazoo, Michigan)).

METHODS

Materials. FeNPs were purchased from SkySpring Nanomaterials, Inc. (Houston, TX) and had a black appearance and a reported diameter of 20−40 nm. The FePVP particles were purchased from U.S. Research Nanomaterials, Inc. (Houston, TX), had an orange appearance, a reported PVP loading of 1% and a diameter of 20−40 nm. The γ-FeNP particles were purchased from US Research Nanomaterials, Inc. (Houston, TX), had an orange appearance and reported diameter of 20−40 nm; these NPs were used as-is. Polystyrenesulfonate sodium salt with MW of 70 000 was purchased from Scientific Polymer Products (Scientific Polymer Products, Inc., Ontario, NY). FePSS particles were prepared by mixing 20 g of γ-FeNP and 15 g of PSS in 1 L of DI water. The pH of the suspension was adjusted to 4.0 using HCL, and was then sonicated in a sonication bat, while being mixed with an immersion mixer for 30 min. The solution was then mixed for additional 18 h, after which the FePSS particles were removed from the suspension using vacuum filtration and poly(ether sulfone) membranes (100 nm) (Membrana, Tokyo, Japan). The particles were then flushed with 3 L of DI water with mixing, and then dried at room temperature for 48 h before being used. The SPW was made with 1.27 M NaCl, 0.165 M $MgCl_2$, 0.018 M KCl, 0.17 M CaCl, and 0.004 M $MgSO_4$, while SSW was prepared with 0.68 M NaCl, 0.03 M $MgCl_2$, 0.013 M CaCl, and 0.019 M $MgSO_4$ all acquired from Fisher Scientific (Thermo Fisher Scientific, Inc., Waltham, MA); the salts were all ACS grade. The Crude Oil was purchased from Texas Raw Crude (Midland, TX). PS-35 and PAN membranes were acquired from Sepro Membranes (Sepro Membranes, Inc., Oceanside, CA) and used as-is. The PVA-CNT membranes were synthesized using a method described elsewhere.[34] Briefly, a solution of 1% 146 000−186 000 MW PVA (Sigma-Aldrich) and multiwall carbon nanotubes functionalized with carboxylic groups (Cheaptubes, Inc., Brattleboro, VT) was prepared in a 3:1 (w/w) ratio. The mixture was pressure filtered (Millipore; Billerica, MA) onto either a PS35 or PAN support with a final CNT loading of 0.63 g/m^2. The composite membrane was then cross-linked in a heated bath (90 °C for 1 h) containing 1 g/L of 50 wt % glutaraldehyde and 0.37 g/L hydrochloric acid (Thermo Fisher Scientific, Inc., Waltham, MA), followed by a drying step in an oven (90 °C for 10 min).

Sample Preparation. Crude oil emulsions were prepared by adding crude oil to 1.5 L of water (DI, SPW or SSW) followed by vigorous mixing using a blender (Oster, Sunbeam Products, Inc.) set at maximum speed for 10 min. The temperature of the solution during the blending was maintained at room temperature using an immersed cooling coil. The prepared emulsion was used as is, unless it was used for the Pickering emulsion preparation. The Pickering emulsion was prepared by adding

FeNPs or FePVP particles to the oil emulsion in a 1:1 (v/w) ratio, followed by mixing with an immersion mixer (built in house) for 1 or 3 h, respectively.

Material Characterization. FeNP and FePVP aggregate size was measured by preparing a 10 mg/L solution in DIW, and measuring the size using a DLS instrument (Brookhaven Instruments; Holtsville, NY) with the detector angle set at 90°. The oil emulsion and Pickering emulsion sizes were measured using optical microscopy images (Thermo Fisher Scientific, Inc., Waltham, MA) and image analysis software (ImageJ); a 0.01 mm calibration slide (AmScope, Irvine, CA) was used to ensure accurate size measurements, with at least 150 oil/Pickering emulsion drops measured. The PVA-CNT films were imaged using SEM (SEM; FEI XL30 SEM-FEG; Hillsboro, OR). SEM samples were attached to an aluminum stub using copper tape. Cross-sectional SEM images were acquired by freezing membranes at −80 °C and then fracturing the surface. Membranes were then sputter coated with Pt/Pd for 30 s. The SEM image of the Pickering emulsion was acquired by placing drops of Pickering emulsion solution onto the aluminum stub and allowing the sample to dry at room temperature overnight; the samples were then sputter coated with Pt/Pd for 40 s. Crude oil contact angle measurements were taken using a contact angle goniometer (Attension; Linthicum Heights, MD) equipped with a polycarbonate inverse cell, where the membrane was attached using Scotch double sided tape (Scotch, Minneapolis, MN), and immersed in DI water for 5 min before allowing a 10 μL oil drop to come in contact with the membrane surface. FeNP and FePVP samples for contact angle measurements were prepared using a method modified from Potapova *et al.*[56−58] In short, 0.1 g/L of FeNP, γ-FeNP, FePSS, and FePVP powder was added to 500 mL of DIW, and the solution was sonicated for 30 min using a horn sonicator (Branson; Danbury, CT). The suspension was then pressure deposited onto a PS35 support at 50 psi and dried at room temperature overnight. The contact angle of the prepared sample was measured with a 0.6 μL water drop in air (Attension; Linthicum Heights, MD).

Filtration System and Fouling Experiments. The filtration experiments were performed with a fully automated membrane filtration system described in more detail elsewhere.[34] Briefly, a cross-flow filtration cell was used, the permeate flow rate (flux) was measured using a scale, and was maintained by adjusting system pressure *via* an electronically controlled valve. Due to the abrasive nature of the NPs used, different pumps had to be used as they failed over time, with a diaphragm pump (Hydra-Cell, Wanner Engineering, Inc., Minneapolis, MN) and a progressive cavity pump (Moyno, Springfield, OH) proving themselves as the only viable options for long-term operations. Other pumps used for short periods included a gear pump (Coleparmer; Vernon Hills, IL) and a rotary vane pump (McMaster-Carr, Chicago, IL). For low temperature experiments, an immersion coil attached to a chiller (Thermo Fisher Scientific, Inc., Waltham, MA) was inserted into the solution tank, and a custom PID controller (Arduino) with a temperature probe in the solution tank was used to maintain constant feed temperature to ±0.25 °C.

All membranes were compressed with DIW at 100 PSI for 12−48 h until constant flux was achieved before experiments began. During the filtration of the Pickering emulsions, the system was operated continuously for 12 h at which point a 5 min cross-flush cleaning event with the feedwater (no pressure) was performed; following the cleaning event, the experiment was resumed. Unless otherwise stated, membrane permeate was returned to the feed tank to maintain constant feed concentrations. During the concentration experiments, the permeate was not returned to the feed and the concentration of the oil was monitored by measuring the volume of permeate produced.

NP Recovery and Reuse. For the FeNP recovery experiments, the Pickering emulsions were prepared by adding 100 mL/L of crude oil to 30 mL of DIW in a 40 mL glass vial followed by sonicating in a bath (Thermo Fisher Scientific, Inc., Waltham, MA) for 10 min. A 1:1 (v/w) ratio of FeNPs was then added to the vial, and the mixture was vigorously mixed using a vortex mixer (Thermo Fisher Scientific, Inc., Waltham, MA) for 1 min. The solution was then transferred to an aluminum boat (42 mL volume, Fisher Scientific) and placed on top of a cylindrical 1 in. × 1 in. N48 neodymium magnet (CMS Magnetics, Garland, TX). The magnet and boat were tipped over perpendicular to the bench, allowing the draining of the water and crude oil, leaving behind a FeNP cake. The FeNP cake was then mixed with a spatula, and Kimwipes (Kimberly-Clark Worldwide, Inc.) were softly pressed against the cake to absorb residual moisture and crude oil, with the wicking process repeated 4−5 times. The alumina boat was then weighted, and a 0.1 g sample was removed and placed on a different aluminum boat, which was then dried at 50 °C for 30 min, weighed, and placed on the N52 magnet once again. Crude oil was then extracted from the 0.1 g sample using 3 consecutive washes with 10 mL of hexane (99% hexanes, Fisher Scientific). The sample was then allowed to dry at 50 °C for 10 min and was weighed one last time; the difference between the dried sample weight and the weight after the hexane wash was used to calculate entrapped oil content in the FeNPs. The reusability of the FeNPs was tested by using the recovered FeNPs (described previously) to stabilize a fresh oil emulsion solution. The same process was followed as above; however, the volume of oil emulsion was adjusted such that the total oil volume of oil emulsion and oil remaining in the NPs would result in a 1:1 (v/w) ratio. The same FeNPs were reused for a total of 3 times, and the overall procedure was duplicated with fresh FeNPs. The oil stabilization was tested by measuring the TOC in the recovered water after magnetic separation, and was always bellow 15 ppm, indicating full stabilization.

Atomic Force Microscopy. Samples for AFM probing were prepared by vortex mixing 0.003 mL/L oil emulsion in a glass vial for 5 min. A glass slide was then held parallel to the bench surface, and 1 mL of the oil emulsion was deposited (using a pipet) on the underside of the glass slide, with the oil emulsion forming a small water drop on the bottom of the glass slide. The slide was allowed to stabilize for 5 min while the oil floats toward the top of the slide and attaches to the glass surface. Then, the slide was carefully inverted and the emulsion solution was replaced with DI water and placed onto the AFM stage (Asylum Research, Santa Barbara, CA). The FeNP stabilized oil droplets were prepared by first coating the slide in oil droplets as described above, and then replacing the DI water with a 0.1 g/L FeNP suspension that had been sonicated with a horn sonicator (Branson; Danbury, CT) for 10 min. The FeNP suspension was allowed to settle onto the oil-coated glass surface for 10 min, and was then flushed out with DI water. For the force probing, triangular tipless tips were used (NP-O10, Bruker, Camarillo, CA) with a reported stiffness of 0.12 N/m. For force measurements, the tips were immersed into a 10 g/L dopamine solution for 10 min before use. The tips were then calibrated by first acquiring the slope from probing the glass surface (getting the V/nm sensitivity) and then by performing a thermal tuning step (measured stiffness values being 0.10 ± 0.01 N/m). To probe the oil drop surface, the tip was aligned over the oil drop using an optical microscope, and then manually lowered onto the surface until the tip engaged. A force profile was then taken with a trigger point being set at 35 nN at a rate of 250 nm/s.

Conflict of Interest: The authors declare no competing financial interest.

Supporting Information Available: The Supporting Information is available free of charge on the ACS Publications website at DOI: 10.1021/acsnano.5b04880.

Performance of PVA-CNT membranes during filtration of crude oil emulsions, energy wells, information on AFM probing of the oil drops and Pickering emulsion drops, and a detailed description of the model (PDF)

Acknowledgment. We appreciate the funding from the IGERT: Water SENSE - Water Social, Engineering, and Natural Sciences Engagement program (Award Abstract No. 1144635), ACS Petroleum Research Fund (54649-DNI9), and the Office of Naval Research (N00014-14-1-0809).

REFERENCES AND NOTES

1. Mohr, S. H.; Wang, J.; Ellem, G.; Ward, J.; Giurco, D. Projection of World Fossil Fuels by Country. *Fuel* **2015**, *141*, 120–135.

2. Benes, J.; Chauvet, M.; Kamenik, O.; Kumhof, M.; Laxton, D.; Mursula, S.; Selody, J. The Future of Oil: Geology versus Technology. *Int. J. Forecast.* **2015**, *31*, 207–221.
3. King, G. M.; Kostka, J. E.; Hazen, T. C.; Sobecky, P. a. Microbial Responses to the Deepwater Horizon Oil Spill: From Coastal Wetlands to the Deep Sea. *Annu. Rev. Mar. Sci.* **2015**, *7*, 377–401.
4. Lee, K.; Cobanli, S. E.; Robinson, B. J.; Wohlgeschaffen, G.; Neff, J. *Produced Water*; Lee, K., Neff, J., Eds.; Springer: New York, NY, 2011.
5. Neff, J. M.; Johnsen, S.; Frost, T. K.; Røe Utvik, T. I.; Durell, G. S. Oil Well Produced Water Discharges to the North Sea. Part II: Comparison of Deployed Mussels (Mytilus Edulis) and the DREAM Model to Predict Ecological Risk. *Mar. Environ. Res.* **2006**, *62*, 224–246.
6. Ekins, P.; Vanner, R.; Firebrace, J. Zero Emissions of Oil in Water from Offshore Oil and Gas Installations: Economic and Environmental Implications. *J. Cleaner Prod.* **2007**, *15*, 1302–1315.
7. Zhang, F.; Zhang, W. B.; Shi, Z.; Wang, D.; Jin, J.; Jiang, L. Nanowire-Haired Inorganic Membranes with Superhydrophilicity and Underwater Ultralow Adhesive Superoleophobicity for High-Efficiency Oil/Water Separation. *Adv. Mater.* **2013**, *25*, 4192–4198.
8. Zhang, W.; Zhu, Y.; Liu, X.; Wang, D.; Li, J.; Jiang, L.; Jin, J. Salt-Induced Fabrication of Superhydrophilic and Underwater Superoleophobic PAA-G-PVDF Membranes for Effective Separation of Oil-in-Water Emulsions. *Angew. Chem., Int. Ed.* **2014**, *53*, 856–860.
9. Ju, J.; Wang, T.; Wang, Q. Superhydrophilic and Underwater Superoleophobic PVDF Membranes via Plasma-Induced Surface PEGDA for Effective Separation of Oil-in-Water Emulsions. *Colloids Surf., A* **2015**, *481*, 151–157.
10. Ejaz Ahmed, F.; Lalia, B. S.; Hilal, N.; Hashaikeh, R. Underwater Superoleophobic Cellulose/electrospun PVDF−HFP Membranes for Efficient Oil/water Separation. *Desalination* **2014**, *344*, 48–54.
11. Zhang, L.; Zhong, Y.; Cha, D.; Wang, P. A Self-Cleaning Underwater Superoleophobic Mesh for Oil-Water Separation. *Sci. Rep.* **2013**, *3*, 2326.
12. Xue, Z.; Wang, S.; Lin, L.; Chen, L.; Liu, M.; Feng, L.; Jiang, L. A Novel Superhydrophilic and Underwater Superoleophobic Hydrogel-Coated Mesh for Oil/Water Separation. *Adv. Mater.* **2011**, *23*, 4270–4273.
13. Liu, N.; Chen, Y.; Lu, F.; Cao, Y.; Xue, Z.; Li, K.; Feng, L.; Wei, Y. Straightforward Oxidation of a Copper Substrate Produces an Underwater Superoleophobic Mesh for Oil/Water Separation. *ChemPhysChem* **2013**, *14*, 3489–3494.
14. Dong, X.; Chen, J.; Ma, Y.; Wang, J.; Chan-Park, M. B.; Liu, X.; Wang, L.; Huang, W.; Chen, P. Superhydrophobic and Superoleophilic Hybrid Foam of Graphene and Carbon Nanotube for Selective Removal of Oils or Organic Solvents from the Surface of Water. *Chem. Commun.* **2012**, *48*, 10660.
15. Gui, X.; Wei, J.; Wang, K.; Cao, A.; Zhu, H.; Jia, Y.; Shu, Q.; Wu, D. Carbon Nanotube Sponges. *Adv. Mater.* **2010**, *22*, 617–621.
16. Zou, J.; Liu, J.; Karakoti, A. S.; Kumar, A.; Joung, D.; Li, Q.; Khondaker, S. I.; Seal, S.; Zhai, L. Ultralight Multiwalled Carbon Nanotube Aerogel. *ACS Nano* **2010**, *4*, 7293–7302.
17. Zhao, Y.; Hu, C.; Hu, Y.; Cheng, H.; Shi, G.; Qu, L. A Versatile, Ultralight, Nitrogen-Doped Graphene Framework. *Angew. Chem., Int. Ed.* **2012**, *51*, 11371–11375.
18. Sun, H.; Xu, Z.; Gao, C. Multifunctional, Ultra-Flyweight, Synergistically Assembled Carbon Aerogels. *Adv. Mater.* **2013**, *25*, 2554–2560.
19. Mecklenburg, M.; Schuchardt, A.; Mishra, Y. K.; Kaps, S.; Adelung, R.; Lotnyk, A.; Kienle, L.; Schulte, K. Aerographite: Ultra Lightweight, Flexible Nanowall, Carbon Microtube Material with Outstanding Mechanical Performance. *Adv. Mater.* **2012**, *24*, 3486–3490.
20. Chakrabarty, B.; Ghoshal, A. K.; Purkait, M. K. Ultrafiltration of Stable Oil-in-Water Emulsion by Polysulfone Membrane. *J. Membr. Sci.* **2008**, *325*, 427–437.
21. Benito, J. M.; Ebel, S.; Gutiérrez, B.; Pazos, C.; Coca, J. No Title. *Water, Air, Soil Pollut.* **2001**, *128*, 181–195.
22. Melle, S.; Lask, M.; Fuller, G. G. Pickering Emulsions with Controllable Stability. *Langmuir* **2005**, *21*, 2158–2162.
23. Kaiser, A.; Liu, T.; Richtering, W.; Schmidt, A. M. Magnetic Capsules and Pickering Emulsions Stabilized by Core−Shell Particles. *Langmuir* **2009**, *25*, 7335–7341.
24. Sacanna, S.; Kegel, W. K.; Philipse, A. P. Thermodynamically Stable Pickering Emulsions. *Phys. Rev. Lett.* **2007**, *98*, 158301.
25. Wang, H.; Lin, K.-Y.; Jing, B.; Krylova, G.; Sigmon, G. E.; McGinn, P.; Zhu, Y.; Na, C. Removal of Oil Droplets from Contaminated Water Using Magnetic Carbon Nanotubes. *Water Res.* **2013**, *47*, 4198–4205.
26. Srijaroonrat, P.; Julien, E.; Aurelle, Y. Unstable Secondary Oil/water Emulsion Treatment Using Ultrafiltration: Fouling Control by Backflushing. *J. Membr. Sci.* **1999**, *159*, 11–20.
27. Nabi, N.; Aimar, P.; Meireles, M. Ultrafiltration of an Olive Oil Emulsion Stabilized by an Anionic Surfactant. *J. Membr. Sci.* **2000**, *166*, 177–188.
28. Zhou, J.; Qiao, X.; Binks, B. P.; Sun, K.; Bai, M.; Li, Y.; Liu, Y. Magnetic Pickering Emulsions Stabilized by Fe 3 O 4 Nanoparticles. *Langmuir* **2011**, *27*, 3308–3316.
29. He, Y.; Wu, F.; Sun, X.; Li, R.; Guo, Y.; Li, C.; Zhang, L.; Xing, F.; Wang, W.; Gao, J. Factors That Affect Pickering Emulsions Stabilized by Graphene Oxide. *ACS Appl. Mater. Interfaces* **2013**, *5*, 4843–4855.
30. Ramsden, W. Separation of Solids in the Surface-Layers of Solutions and "Suspensions" (Observations on Surface-Membranes, Bubbles, Emulsions, and Mechanical Coagulation). -- Preliminary Account. *Proc. R. Soc. London* **1903**, *72*, 156–164.
31. Pickering, S. U. CXCVI. - Emulsions. *J. Chem. Soc., Trans.* **1907**, *91*, 2001–2021.
32. Vignati, E.; Piazza, R.; Lockhart, T. P. Pickering Emulsions: Interfacial Tension, Colloidal Layer Morphology, and Trapped-Particle Motion. *Langmuir* **2003**, *19*, 6650–6656.
33. Demond, A. H.; Lindner, A. S. Estimation of Interfacial Tension between Organic Liquids and Water. *Environ. Sci. Technol.* **1993**, *27*, 2318–2331.
34. Dudchenko, A. V.; Rolf, J.; Russell, K.; Duan, W.; Jassby, D. Organic Fouling Inhibition on Electrically Conducting Carbon Nanotube−polyvinyl Alcohol Composite Ultrafiltration Membranes. *J. Membr. Sci.* **2014**, *468*, 1–10.
35. Van den Brink, P.; Zwijnenburg, A.; Smith, G.; Temmink, H.; van Loosdrecht, M. Effect of Free Calcium Concentration and Ionic Strength on Alginate Fouling in Cross-Flow Membrane Filtration. *J. Membr. Sci.* **2009**, *345*, 207–216.
36. Ye, Y.; Clech, P. Le; Chen, V.; Fane, A. G. Evolution of Fouling during Crossflow Filtration of Model EPS Solutions. *J. Membr. Sci.* **2005**, *264*, 190–199.
37. Defrance, L.; Jaffrin, M. Comparison between Filtrations at Fixed Transmembrane Pressure and Fixed Permeate Flux: Application to a Membrane Bioreactor Used for Wastewater Treatment. *J. Membr. Sci.* **1999**, *152*, 203–210.
38. Munz, M.; Mills, T. Size Dependence of Shape and Stiffness of Single Sessile Oil Nanodroplets As Measured by Atomic Force Microscopy. *Langmuir* **2014**, *30*, 4243–4252.
39. Singh, G.; Song, L. Experimental Correlations of pH and Ionic Strength Effects on the Colloidal Fouling Potential of Silica Nanoparticles in Crossflow Ultrafiltration. *J. Membr. Sci.* **2007**, *303*, 112–118.
40. Lohwacharin, J.; Takizawa, S. Effects of Nanoparticles on the Ultrafiltration of Surface Water. *J. Membr. Sci.* **2009**, *326*, 354–362.
41. Springer, F.; Laborie, S.; Guigui, C. Removal of SiO2 Nanoparticles from Industry Wastewaters and Subsurface Waters by Ultrafiltration: Investigation of Process Efficiency, Deposit Properties and Fouling Mechanism. *Sep. Purif. Technol.* **2013**, *108*, 6–14.
42. Lin, S.; Cheng, Y.; Liu, J.; Wiesner, M. R. Polymeric Coatings on Silver Nanoparticles Hinder Autoaggregation but Enhance Attachment to Uncoated Surfaces. *Langmuir* **2012**, *28*, 4178–4186.
43. Wan, L.-S.; Xu, Z.-K.; Wang, Z.-G. Leaching of PVP from polyacrylonitrile/PVP Blending Membranes: A Comparative

Study of Asymmetric and Dense Membranes. *J. Polym. Sci., Part B: Polym. Phys.* **2006**, *44*, 1490–1498.
44. Jung, B.; Yoon, J. K.; Kim, B.; Rhee, H.-W. Effect of Molecular Weight of Polymeric Additives on Formation, Permeation Properties and Hypochlorite Treatment of Asymmetric Polyacrylonitrile Membranes. *J. Membr. Sci.* **2004**, *243*, 45–57.
45. Aveyard, R.; Binks, B. P.; Clint, J. H. Emulsions Stabilised Solely by Colloidal Particles. *Adv. Colloid Interface Sci.* **2003**, *100−102*, 503–546.
46. Aveyard, R.; Clint, J. H.; Horozov, T. S. Aspects of the Stabilisation of Emulsions by Solid Particles: Effects of Line Tension and Monolayer Curvature Energy. *Phys. Chem. Chem. Phys.* **2003**, *5*, 2398.
47. Torkzaban, S.; Bradford, S. a.; Walker, S. L. Resolving the Coupled Effects of Hydrodynamics and DLVO Forces on Colloid Attachment in Porous Media. *Langmuir* **2007**, *23*, 9652–9660.
48. Bergendahl, J.; Grasso, D. Prediction of Colloid Detachment in a Model Porous Media: Hydrodynamics. *Chem. Eng. Sci.* **2000**, *55*, 1523–1532.
49. Johnson, K. L.; Kendall, K.; Roberts, A. D. Surface Energy and the Contact of Elastic Solids. *Proc. R. Soc. London, Ser. A* **1971**, *324*, 301–313.
50. Bai, R.; Tien, C. Particle Detachment in Deep Bed Filtration. *J. Colloid Interface Sci.* **1997**, *186*, 307–317.
51. Chan, S. K.; Ng, K. M. Geometrical Characteristics of the Pore Space in a Random Packing of Equal Spheres. *Powder Technol.* **1988**, *54*, 147–155.
52. Schrader, M. E. Young-Dupre Revisited. *Langmuir* **1995**, *11*, 3585–3589.
53. Office, U. G. P. 33 CFR 155.350−370; Oily Mixture (bilge Slops) Discharges on Oceangoing Ships, Excluding Ships That Carry Ballast Water in Their Fuel Oil Tanks; **2010**; pp 350−370.
54. Chew, C. M.; Aroua, M. K.; Hussain, M. a.; Ismail, W. M. Z. W. Practical Performance Analysis of an Industrial-Scale Ultrafiltration Membrane Water Treatment Plant. *J. Taiwan Inst. Chem. Eng.* **2015**, *46*, 132–139.
55. Pearce, G. K. UF/MF Pre-Treatment to RO in Seawater and Wastewater Reuse Applications: A Comparison of Energy Costs. *Desalination* **2008**, *222*, 66–73.
56. Potapova, E.; Yang, X.; Westerstrand, M.; Grahn, M.; Holmgren, a.; Hedlund, J. Interfacial Properties of Natural Magnetite Particles Compared with Their Synthetic Analogue. *Miner. Eng.* **2012**, *36−38*, 187–194.
57. Potapova, E.; Yang, X.; Grahn, M.; Holmgren, A.; Forsmo, S. P. E.; Fredriksson, A.; Hedlund, J. The Effect of Calcium Ions, Sodium Silicate and Surfactant on Charge and Wettability of Magnetite. *Colloids Surf., A* **2011**, *386*, 79–86.
58. Potapova, E.; Grahn, M.; Holmgren, A.; Hedlund, J. The Effect of Polymer Adsorption on the Wetting Properties of Partially Hydrophobized Magnetite. *J. Colloid Interface Sci.* **2012**, *367*, 478–484.